

## A Study of South Asian Monsoon Energetics

T. N. KRISHNAMURTI, M. C. SINHA, BHASKAR JHA, AND U. C. MOHANTY\*

*Department of Meteorology, The Florida State University, Tallahassee, Florida*

(Manuscript received 12 September 1996, in final form 5 December 1997)

### ABSTRACT

Monsoon forecasting is one of the most difficult components of the global weather prediction problem. The operational forecasts over the Asian monsoon region are known to have useful skill only for roughly 2–3 days. The rapid deterioration of monsoon forecasts can be attributed to a number of factors such as data deficiencies, physical parameterization in the forecast models, and representation of orography and surface boundary conditions, such as details of sea surface temperature, snow cover, etc. The study of energetics of the model output helps in understanding the above problems. This study is aimed toward the examination of the monsoon energetics. Here it is shown that the use of kinetic energies of the rotational and divergent motions have a special advantage. In order to show these features in the maintenance of a fully developed monsoon, the authors have taken the results of a global model. Such a model is internally consistent and given a reasonable forecast of the motion, thermal, and precipitation fields, the authors believe that such a model-generated dataset can provide useful insights. Direct use of observations and their analysis make it difficult to perform such studies because of data voids and the data errors and inconsistencies. Models tend to produce somewhat more consistent fields during the course of short-range prediction. Although the results obtained contain a model bias, the authors nevertheless performed short-range forecasts with a high-resolution global model and rely only on these if the forecasts appear to be quite reasonable.

The Florida State University Global Spectral Model at the resolution T170 (170 waves triangular truncation) was run to carry out several experiments to investigate the issue of the maintenance of the Asian monsoon. In this context the authors examined the issue of the maintenance of the monsoon over a south Asian domain. The computations show that differential heating (i.e., the covariance of heating and temperature) leads to the growth of available potential energy, which is next passed on to the divergent motions via the covariance of vertical velocity and temperature. The final link in this scenario is the transfer of energy from the divergent to the rotational part of the motion field that describes the monsoon. These are largely described by  $\psi$ - $\chi$  interaction via the covariance of  $\nabla\psi$  and  $\nabla\chi$  (where  $\psi$  is a streamfunction and  $\chi$  is a velocity potential). It is noted that lateral boundary fluxes are also important for the maintenance of the monsoon. Lateral coupling with the monsoon of southeast Asia and with the Southern Hemispheric circulation are also some of the crucial elements of the overall energetics.

### 1. Introduction

The scope of this paper is on monsoon energetics during its mature phase. The energetics of monsoon, where the rotational and divergent circulations are explicitly represented, is a unique aspect of this study. This formalism brings in the role of differential heating, the generation of available potential energy, its transformation to divergent kinetic energy, and the eventual maintenance of the monsoon via interactions among the divergent and rotational components. Computation of

the energetics of an open system, such as the monsoon, is a difficult exercise due to data limitations and inherent errors of budget estimates. In the context of global model prediction of the monsoon, this difficulty can be somewhat alleviated. It is quite difficult to provide residue-free budgets of atmospheric energetics, due to the difficulties of handling quadratic and triple product terms consistent with the overall model structure (Wiin-Nielson and Chen 1993). Furthermore, because of the semi-implicit time differencing and the methodology of the spectral transform used in the global spectral model, closed-form calculations of atmospheric energetics are not easy to formulate. The present paper approaches the issue of the maintenance of a mature monsoon system from a database that was generated from relatively successful predictions of the circulations and precipitation. We have used a similar approach for studies on hurricane formation (Krishnamurti et al. 1994). It is difficult to see the maintenance of the monsoon from a string of analyzed fields. The spinup of the monsoon using a

---

\* Current affiliation: The Center for Atmospheric Sciences, Indian Institute of Technology, New Delhi, India.

---

*Corresponding author address:* Dr. T. N. Krishnamurti, Dept. of Meteorology, The Florida State University, Tallahassee, FL 32306-4520.  
E-mail: tnk@io.met.fsu.edu

high-resolution global model appears to produce a better picture. A model run with reasonable forecasts is able to describe the above sequence very clearly. The budgets of the energetics are performed carefully, but they are not entirely residue free.

Monsoon research has moved in several areas encompassing many time and space scales, ranging from the diurnal to the interannual. Energetics provide a consistency check for many data analysis and modeling results. The proposed energy transformations using the divergent and rotational components as a frame of reference appears to be important for large thermally driven systems such as the monsoon. If the simulations or prediction of large-scale variables monsoon appear reasonable compared to observations then there is some hope that we could obtain a better understanding of such a system from a detailed diagnosis of the energy transformation. Given the interplay between the land and ocean, between the convective heating over the precipitating areas and of the radiative cooling over the large surrounding nonprecipitating areas, between the generation of available potential energy and its conversions to the kinetic energy of the motion fields, and between the nondivergent components of the motion field of the large monsoonal flows and the divergent gyres on the vertical planes the Hadley and Walker type overturnings, the proposed energetics appears to be well suited for monsoon diagnosis.

An important advance in the energetics of the monsoon comes from a logical extension of the zonally symmetric monsoon to a full three dimensions. This concept is further developed to show the use of energy equations in terms of rotational and divergent motions. This extension provides a very useful three-dimensional framework for the understanding of the monsoon. This approach enables us to show a simple stream for the workings of the monsoon. The differential heating first builds the available potential energy of the monsoon system, the Hadley and Walker circulations then pass this energy on to the divergent motions, and nonlinear interactions among the divergent and rotational motions pass this on to the rotational motion resulting in the maintenance of the monsoon. These ideas are common to both the zonally symmetric and the fully three-dimensional monsoon. Although some of these ideas were previously expressed in Krishnamurti (1985), the present study has carried these notions of energy transformations to some degree of completeness.

## 2. Maintenance of a monsoon system

In this section we shall present the framework for the monsoon energetics. We shall first present the energetics for the zonally symmetric monsoon.

### a. Zonally symmetric monsoon

One of the most powerful frameworks for the understanding of the monsoon behavior is the energetics

TABLE 1. List of symbols.

$u$	Eastward wind component
$t$	Time
$v$	Northward wind component
$\omega$	Vertical wind component
$p$	Pressure
$f$	Coriolis parameter
$T$	Temperature
$g$	Acceleration due to gravity
$R$	Gas constant for dry air
$c_p$	Specific heat of air at constant pressure
$q$	Specific humidity
$F_x$	Eastward frictional force
$F_y$	Northward frictional force
$E$	Evaporation
$P$	Potential energy
$K$	Kinetic energy
$\psi$	Streamfunction velocity potential
$D$	Dissipation of energy
$B$	Boundary fluxes
$G$	Generation of energy
$z$	Geopotential height
$\nabla$	Horizontal gradient operator
$\Sigma H_i$	Diabatic heating (radiative, convective, large-scale condensation, etc.)
$P_r$	Precipitation
$D_p$	Dissipation of potential energy
$B_p$	Boundary flux of potential energy

based on a zonally symmetric model; see Murakami et al. (1970), where they described the monsoon by the following equations. (A list of symbols is provided in Table 1.)

Zonal equation of motion:

$$\frac{\partial u}{\partial t} = -v \frac{\partial u}{\partial y} - \omega \frac{\partial u}{\partial p} + fv + F_x; \quad (1)$$

Meridional equation of motion:

$$\frac{\partial v}{\partial t} = -v \frac{\partial v}{\partial y} - \omega \frac{\partial v}{\partial p} - fu - g \frac{\partial z}{\partial y} + F_y; \quad (2)$$

Equation of continuity:

$$\frac{\partial v}{\partial y} + \frac{\partial \omega}{\partial p} = 0; \quad (3)$$

First law of thermodynamics:

$$\frac{\partial T}{\partial t} = -v \frac{\partial T}{\partial y} - \omega \frac{\partial T}{\partial p} - \frac{RT}{c_p p} \omega + \sum \frac{H_i}{c_p}; \quad (4)$$

Moisture conservation:

$$\frac{\partial q}{\partial t} = -v \frac{\partial q}{\partial y} - \omega \frac{\partial q}{\partial p} + E - P_r. \quad (5)$$

This zonally symmetric system has several interesting properties. Since the meridional wind  $v$  is uniquely de-

terminated from the vertical velocity  $\omega$  (mass continuity equation), the meridional wind is entirely divergent. Furthermore, since the estimation of the vertical velocity  $\omega$  [Eq. (3)] does not depend on the zonal velocity  $u$ , the latter is entirely nondivergent.

The energetics of this system describe exchanges among the divergent and the rotational energy components. The energy equations are as follows.

Zonal kinetic energy (rotational kinetic energy):

$$\frac{\partial K}{\partial t} \psi = \langle K_\chi, K_\psi \rangle - D_\chi + B_\psi; \quad (6)$$

Meridional kinetic energy (divergent kinetic energy):

$$\frac{\partial K}{\partial t} \chi = -\langle K_\chi, K_\psi \rangle + \langle P, K_\chi \rangle - D_\chi + B_\chi; \quad (7)$$

Internal plus potential energy:

$$\frac{\partial P}{\partial t} = -\langle P, K_\chi \rangle + G - D_p + B_p. \quad (8)$$

Here  $D$  denotes dissipations and  $B$  denotes boundary flux terms, which are absent in the symmetric global system.

The above equations describe the energetics of this system. The energy quantities are integrals over a closed domain, that is,

$$\int (\ ) dm = \frac{1}{g} \int_p \int_y (\ ) dy dp, \quad (9)$$

where the  $y$  integral covers a closed meridional domain and the  $p$  integral covers the entire vertical column of the atmosphere. The bracketed terms denote an energy exchange from the first to the second member. In the absence of dissipation ( $D_\psi$ ,  $D_p$ , and  $D_\chi$ ), boundary fluxes ( $B_\psi$ ,  $B_\chi$ ,  $B_p$ ), and generation  $G$ , the total energy (zonal kinetic energy  $K_\psi$  + meridional kinetic energy  $K_\chi$  + internal and potential energy of the system  $P$ ) is an invariant over the closed domain.

The maintenance of a statistically steady monsoon is described by the following inequality statements (Krishnamurti 1985).

- 1) In a statistical steady state,  $(\partial/\partial t)K_\chi$  is small and frictional dissipation of zonal kinetic energy  $-D_\psi$  is  $<0$ , hence there must exist an energy exchange from the meridional (divergent) to the zonal (rotational) kinetic energy; that is,  $\langle K_\chi, K_\psi \rangle$  must be positive.
- 2) In a statistical steady state,  $(\partial/\partial t)K_\chi$  is small and frictional dissipation of meridional kinetic energy  $-D_\chi$  is negative; furthermore  $-\langle K_\chi, K_\psi \rangle$  is negative, hence there must exist an energy exchange from internal plus potential energy to meridional kinetic energy; that is,  $\langle P, K_\chi \rangle$  must be positive.
- 3) A net dissipation of internal plus potential energy,  $-D_p < 0$ , plus the fact that  $-\langle P, K_\chi \rangle$  is negative,

requires that in a near-steady-state system there must be a net generation of energy  $G$  to maintain the system.

Here  $G$  denotes differential heating, which is in fact a covariance of the diabatic heating rate  $H$  and the temperature. Thus the maintenance of a steady-state monsoon [ $(\partial/\partial t)K_\psi \approx 0.0$ ] requires a net barotropic energy exchange  $\langle K_\chi, K_\psi \rangle$ , which in turn requires a net Hadley-type overturning  $\langle P, K_\chi \rangle$  and is facilitated by a differential heating,  $G$ , that drives this system.

Murakami et al. (1970) simulated a near-steady-state monsoon in a zonally symmetric framework. That monsoon simulation contained several features of the monsoon, such as the southern trades, the Mascarene high, cross-equatorial flow, the southwest monsoon, the monsoon trough, the monsoon rains near  $20^\circ\text{N}$ , the warm troposphere above the monsoon trough, the Tibetan high, and the tropical easterly jet stream. These are the main elements of the monsoon system as identified by Krishnamurti and Bhalme (1976).

It is worth mentioning that a statistically steady monsoon is here interpreted in a broader time-averaged context. Within this period one can in fact have short spells of dry and wet periods regionally. This time-averaged period is not like a preonset or a postonset period when the monsoon rainfall over the entire region is quite deficient. It is meant to imply averages over periods of the order of a week.

### b. Three-dimensional energetics

The three-dimensional counterpart of the above framework are the vorticity, divergence, mass continuity, and the thermal and moisture conservation equations. This system was described in Krishnamurti and Ramanathan (1982). The operation of  $\mathbf{k} \cdot \nabla \chi$  on the equations of motion is used to obtain the vorticity equation. That operation removes the pressure gradient term in the vorticity equation. Thus it is possible to obtain very robust energy transformation equations for the three-dimensional case. As for the zonally symmetric case, the absence of a pressure gradient term in the corresponding rotational kinetic energy equation provides the useful decoupling for a similar interpretation of the monsoon system as in three dimensions. The three-dimensional energy equations are as follows.

Rotational kinetic energy:

$$\frac{\partial K_\psi}{\partial t} = \langle K_\chi, K_\psi \rangle - D_\psi + B_\psi; \quad (10)$$

Divergent kinetic energy:

$$\frac{\partial K_\chi}{\partial t} = \langle P, K_\chi \rangle - \langle K_\chi, K_\psi \rangle - D_\chi + B_\chi; \quad (11)$$

Internal plus potential energy:

$$\frac{\partial P}{\partial t} = -\langle P, K_\chi \rangle + G - D_p + B_p. \quad (12)$$

Here, the energy exchange terms  $\langle K_\chi, K_\psi \rangle$  and  $\langle P, K_\chi \rangle$  are

$$\begin{aligned} \langle K_\chi, K_\psi \rangle = & f \nabla \psi \cdot \nabla \chi + \nabla^2 \psi (\nabla \psi \cdot \nabla \chi) \\ & + \omega J \left( \psi, \frac{\partial \chi}{\partial p} \right) + \nabla^2 \chi \frac{(\nabla \psi)^2}{2}, \end{aligned} \quad (13)$$

$$\langle P, K_\chi \rangle = -\chi g \nabla^2 z. \quad (14)$$

The details of these  $\chi$ - $\psi$  interactions are given in appendix A. The interpretation of this system is exactly analogous to that of the zonally symmetric system. The maintenance of monsoon can be attributed to the energy it receives from the divergent motions, the Hadley-Walker-type vertical overturning, and the differential heating.

### 3. Sample monsoon forecast—Synoptic features

The framework for this study is the FSU<sup>1</sup> global spectral model and is outlined in appendix B. This is a high-resolution model with a horizontal resolution of 170 waves (triangular truncation) and 15 vertical layers. The model includes the spectral transform method (for the computation of the nonlinear terms and the physical processes) and the semi-implicit time-differencing algorithm. The model includes a comprehensive array of physical processes, that is, parameterization of dry, shallow, and deep convection; interactive cloud radiative processes; surface energy balance (diurnal change); surface hydrology; surface similarity fluxes; planetary boundary layer; air-sea interactions; effects of snow; and ice cover and envelope orography. The model includes a physical initialization phase that enables us to initialize the rain rates (Krishnamurti et al. 1991; Krishnamurti et al. 1993; Krishnamurti et al. 1994).

The present study examines the energetics of a monsoon forecast during the 6-day period 2–7 August 1979, when the intensity and precipitation of the monsoon appeared to be quite steady over the regions of the Indian Monsoon (Krishnamurti et al. 1990). We illustrate the steady-state nature of the basic energy parameters in section 4a.

#### a. Datasets

The main datasets for this study came from the final FGGE IIIb analysis of ECMWF, which were archived at a horizontal resolution of 1.875° latitude/longitude; these were derived from a spectral model at the resolution T63 (a list of acronyms is provided in Table 2).

TABLE 2. List of acronyms.

FSU	Florida State University
T170	170 waves triangular truncation
FGGE IIIb	First GARP Global Experiment Level III b
GARP	Global Atmospheric Research Program
ECMWF	European Centre for Medium-Range Weather Forecasts
FGGE/MONEX	FGGE/Monsoon (special observation period) Experiment
OLR	outgoing longwave radiation
SSM/I	Special Sensor Microwave Imager

These datasets were subjected to physical initialization using the FGGE/MONEX rainfall based on raingauge and OLR datasets. Our rain-rate algorithm is described in Krishnamurti et al. (1983b).

#### b. Case study, observed features

The large-scale synoptic situation during this week of active monsoon, 2–7 August 1979, was rather typical. At 850 hPa, Fig. 1 (left panel) shows the flow features, which include the southern trades (with amplitude around 10 m s<sup>-1</sup>), the cross-equatorial flow near the Kenya Coast, the Somali jet (with amplitude around 20 to 25 m s<sup>-1</sup>), the westerly monsoon current over India, and the monsoon trough along 20°N. During this period a weak tropical depression moved westward from the northern Bay of Bengal, which strengthened the moist monsoon flows over the Indian monsoon region. This resulted in an active monsoon spell with rainfall amounts in excess of 100 mm day<sup>-1</sup> over the west coast of India, the northern Bay of Bengal, and the Burmese coast. The westward motion of an active monsoon disturbance enhanced the divergent motions, which in turn appeared to provide a proper alignment of the velocity potential and the streamfunction for energy exchange from divergent to rotational kinetic energy ( $\chi$ - $\psi$  interaction), which is an area of emphasis in this paper. This will become apparent from our analysis of  $\psi$ - $\chi$  interactions, which are discussed in section 4f (particularly in reference to the energy exchanges portrayed there; i.e., Fig. 10).

The upper-tropospheric circulation at 200 hPa, shown in Fig. 2 (left panel) also exhibits what we might call typical features. An east-northeasterly tropical jet with an amplitude of roughly 30 m s<sup>-1</sup> prevailed between 20°N and 10°S. The return flow toward the east occurred near 20°S. The upper-tropospheric anticyclone was located near 25°N. During this active spell of the monsoon, the 200-hPa flow did not exhibit any unusual features. However, this seemingly climatological pattern at 200 hPa did convey interesting properties in its relative description of the divergent and rotational motions, which were also central for the maintenance of the monsoon.

<sup>1</sup> Acronyms are defined in Table 2.

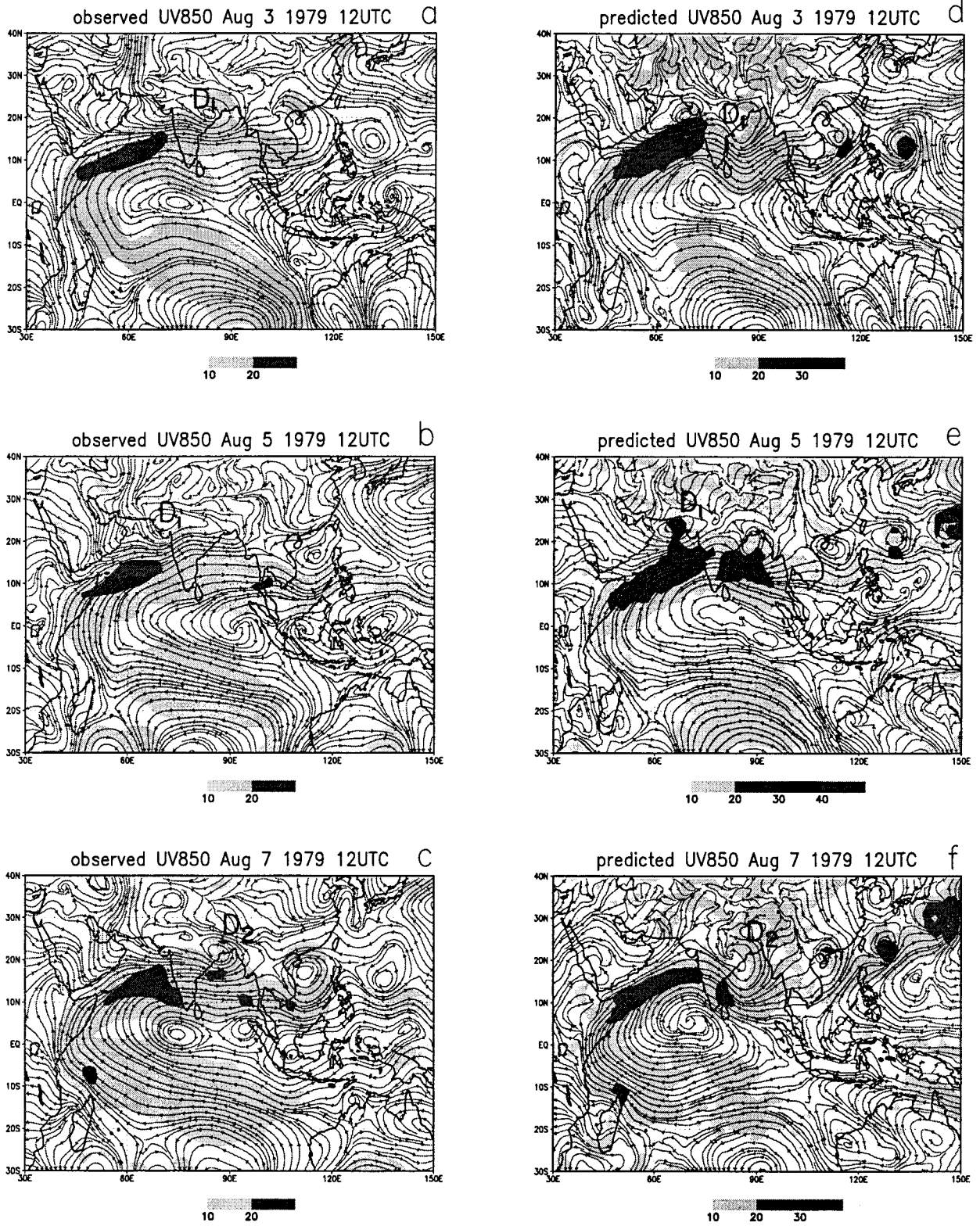


FIG. 1. 850-mb streamlines and isotachs (shaded). Left panel: observed wind field for 3, 5, and 7 August 1979 at 1200 UTC. Right panel: Predicted wind field for 3, 5, and 7 August 1979 at 1200 UTC. (Note initial date of forecast is 2 August 1979 at 1200 UTC). Units:  $m s^{-1}$ ; shaded area indicates wind speed according to the scale shown below each figure.

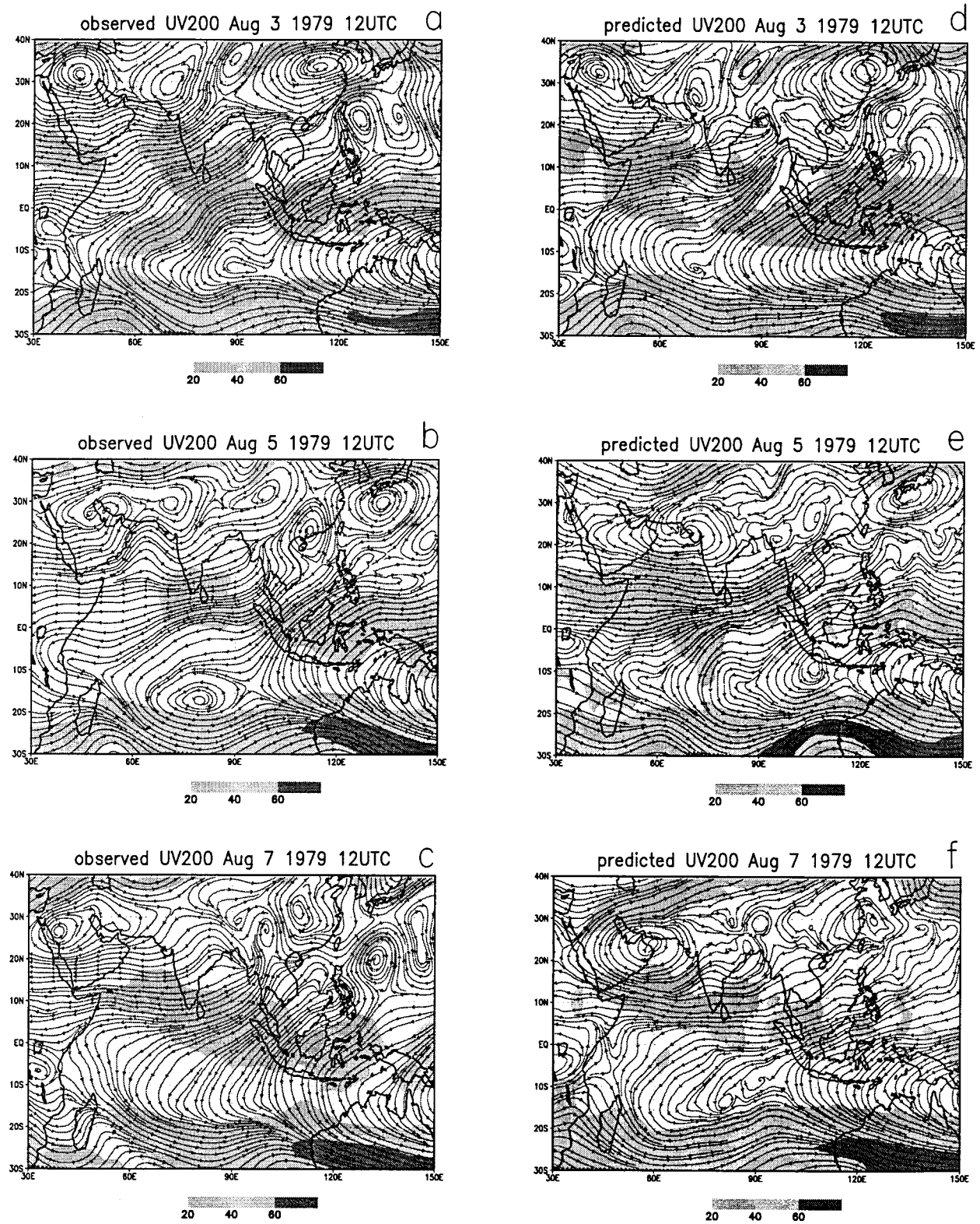


FIG. 2. 200-mb streamlines and isotachs (shaded). Left panel: observed wind field for 3, 5, and 7 August 1979 at 1200 UTC. Right panel: Predicted wind field for 3, 5, and 7 August 1979 at UTC. (Note, initial data of forecast is 2 August 1979 at 1200 UTC). Units:  $m s^{-1}$ ; shaded area indicates wind speed according to the scale shown below each figure.

### c. Predicted fields

A 5-day forecast was made with the global model. The forecast features were as follows. The predicted fields at 850 and 200 hPa are shown in the right panels of Figs. 1 and 2. Here the observed and predicted charts are for days 1, 3, and 5. The monsoon trough was located along 20°N. A monsoon depression moves rapidly from the Bay of Bengal to western India between days 1 and 3. On day 5 another monsoon depression forms at the head of the Bay of Bengal. The model predictions depict these features quite accurately. A series of alternating cyclonic and anticyclonic systems along 30°S are very well predicted through the first 5 days of the forecast. The main features of the monsoon circulations, such as the southern trades, monsoon westerlies, southern equatorial trough, and the cross-equatorial flow off the Kenya coast are reasonably simulated.

At 200 hPa the overall circulations are predicted reasonably through day 5 of the forecast. The forecast failed to predict an upper low to the northeast of the Philippine Islands. The model predictions of the subtropical jet near 25°S were quite successful. The tropical easterly jet near 5°N was reasonably handled by the model. Although the model predicted a family of anticyclonic eddies near 25°N, their locations were not very accurately placed. That is partly related to the fact that wind speeds over the region are very weak and the demands on accurate streamline analysis require a high accuracy on the low wind speeds,  $<5 \text{ m s}^{-1}$ , in order to portray the locations of the anticyclonic outflow centers.

### d. Precipitation forecasts

In the context of the model energetics, the quality of the predictions and the distribution of rainfall are of interest. In Fig. 3 we illustrate the “observed” and the predicted mean of 120 h of the forecast in units of  $\text{mm day}^{-1}$ . The observed rain is based on an OLR rain-rate algorithm (Krishnamurti et al. 1983b). An axis of heavy rain extends zonally along 20°N over the land mass of the Asian monsoon. Heaviest monsoon rainfall occurred over the west coast of India, northeast India, Bangladesh, Burma, and adjoining Bay of Bengal. A disturbance moved over north India from the Bay of Bengal, bringing in very heavy rains ( $137 \text{ mm day}^{-1}$ ) over Bengal and persistent heavy rainfall over the northern part of the west coast of India.

The predicted maxima of rain at resolution T170 were generally higher than the observed OLR-based estimates. The observed rain based on OLR datasets were on a  $1^\circ$  lat by  $1^\circ$  long resolution, whereas the separation of the transform grid points near 20°N of the forecast model at resolution T170 is of the order of 70 km. Overall the forecasts capture the maximum rainfall over the west coast of India, north and central India, the Bengal region, the Burmese coast, and the typhoon rain-

fall over the western Pacific Ocean. During this period two typhoons were active over the western Pacific Ocean (Krishnamurti and Oosterhof 1989). Given this quality of rainfall prediction, we expect the model to describe the generation of available potential energy from the latent heating reasonably during the first 5 days of the forecast. Although the predicted intensity of rainfall is higher than the OLR-based estimates, the model budget of the energetics would be consistent with respect to these higher rainfall amounts. Perhaps the following needs to be said about the OLR-based rainfall estimates. Low values of OLR are often seen over regions where the observed (raingauge-based rainfall) amounts are considerably less. We believe that cirrus decks spread southwestward from land areas, especially the Burmese coast of the Bay of Bengal and the southwest coast of India, where the tropical easterly jet spreads the cirrus toward the ocean. This can often lead to offshore rainfall maxima. We have noted between OLR-based and the microwave radiometer-based satellite estimates over these regions. We believe that the some of the differences between the model and the OLR-based estimates may be related to this problem. The topic of the offshore rainfall has drawn some attention in recent years (Ogura and Yoshizaki 1988; Smith and Lin 1983). At first several scientists felt that this OLR-based offshore rainfall might have been a mislocation, when in fact this is orographic rainfall occurring inland and closer to the coast. However, an issue of offshore rainfall does appear to be real and is confirmed by more recent SSM/I-based rainfall estimates.

## 4. Energy transformations

In this section we shall present the results of the transfer from available potential energy to divergent and rotational components of kinetic energy and maintenance of a near-steady monsoon circulation with a number of quasi-permanent features associated with it.

In the subsections to follow, reference should be made to appendix A, where the framework for the energy quantities and the energy transformations are outlined. While the subsections might appear somewhat unsystematic, they are presented to convey the essential findings, and the summary provides a synthesis.

### a. Maintenance of monsoon

In this study we have deliberately taken an active monsoon episode where the behavior of monsoon between 30°S and 40°N, 30° and 150°E exhibits many of the monsoon features such as the southern trades, the southwest monsoon flows over the Arabian sea, the total rainfall over India, the upper-tropospheric tropical easterly jet, and the monsoon trough, that is, the low pressure system over northern India.

In Figs. 4a–c we show the day-to-day change in the domain-averaged rotational and divergent kinetic en-

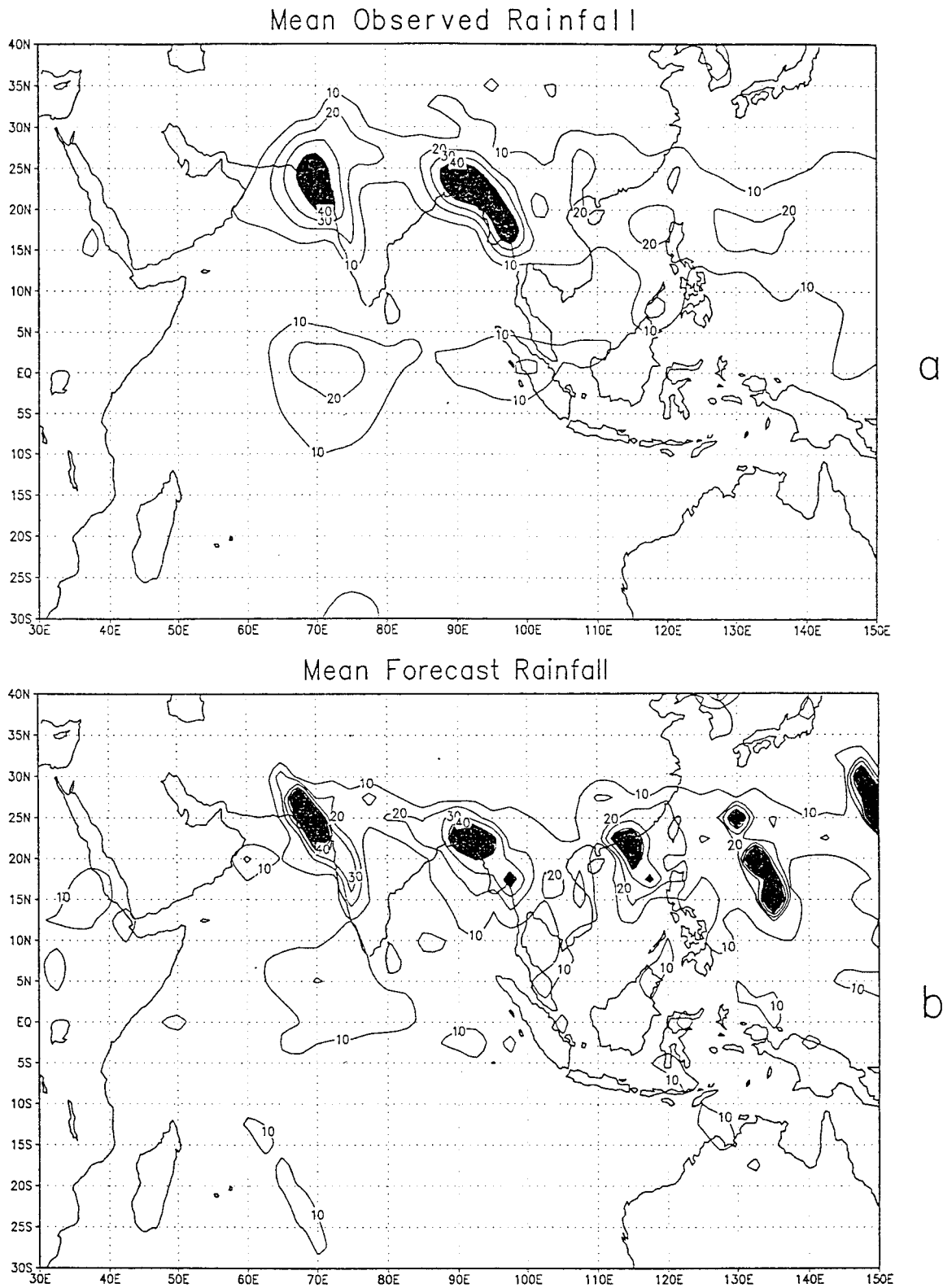


FIG. 3. Mean rainfall for the period 3–7 August 1979. Units  $\text{mm day}^{-1}$ . Top panel: based on observations; bottom panel: based on model forecasts.

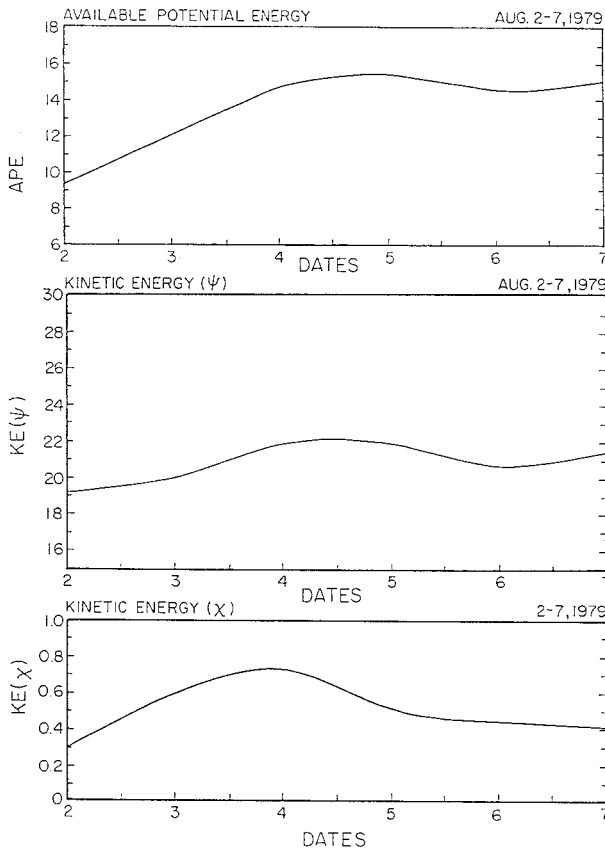


FIG. 4. Average energy quantities over a monsoon domain, 30°S–40°N, 30°–150°E, and between 100 and 1000 hPa surfaces. Units  $\text{m}^2 \text{s}^{-2}$ . (a) Available potential energy, (b) rotational kinetic energy, and (c) divergent kinetic energy.

ergy and available potential energy. The domain extends from 30° to 150°E, from 30°S to 40°N, and from 100 to 1000 hPa along the vertical. The energy quantities are defined by the relations

$$K_{\psi} = \frac{1}{g} \int_p \int_y \int_x \frac{(u_{\psi}^2 + v_{\psi}^2)}{2} dx dy dp,$$

$$K_x = \frac{1}{g} \int_p \int_y \int_x \frac{(u_x^2 + v_x^2)}{2} dx dy dp,$$

and

$$\text{APE} = \frac{1}{g} \int_p \frac{\bar{T}}{\gamma_d - \bar{\gamma}} \left[ \overline{\left[ \frac{T'}{\bar{T}} \right]^2} \right] dp.$$

Except for the kinetic energy of divergent flow, these basic energy quantities exhibit day-to-day variations within a small percentage of their mean value, especially after day 2 of this forecast. This implies that the internal generation and transfer processes, frictional dissipation, and boundary fluxes maintain this near balance.

### b. The overall energetics and maintenance of the monsoon

Figure 5 illustrates the overall energetics of the monsoon. All units in this diagram are  $10^{-5} \text{ m}^2 \text{ s}^{-3}$ . Each box in this diagram is an average value of the respective energy transformation (or tendency) over a domain 30°–150°E, 30°S–40°N and between 100 and 1000 hPa. This energetics cover the period 2–7 August 1979.

We shall describe this illustration consistent with the discussion of section 2. The salient energy source is the generation of available potential energy  $G$ , which has a value of 47.3 units. This generation over the monsoon domain arises from the covariance of the elements of diabatic heating and the thermal distribution. This generation includes the contributions from the domain Hadley cell as well as the eddy motions. When the monsoon is nearly steady and robust, the large contributors to this heat come from the release of latent heating over the heavy rain areas. In this example, that region was located over the northern Bay of Bengal and the region to the north of it. The predicted rainfall of this period was illustrated in Fig. 3. The other components of heating that contribute to this generation include the radiative flux convergence and the sensible heat fluxes from the land and ocean surfaces. The convective heating in the rain areas is much larger than the radiative component. In the rain-free areas of the southern oceans, the tropospheric thermal field is relatively cold. Therefore the covariance of radiative cooling and the colder temperatures also contributes substantially to a net generation of available potential energy over this domain.

In Fig. 6 we illustrate the components of the overall generation. These are again integrated over the entire monsoon domain and averaged over 6 days. The standard errors for such calculations of energy transformations are usually large if atmospheric data are used (Saltzman 1970). However, if one uses the model-generated data and performs energy transformation consistently, the errors are much reduced. Here we note that the largest contributions to the generation arise from the radiative heating and are followed next by the contributions from cumulus convection. The contribution to the generation from large-scale condensation heating is small. The diffusion effects are substantial and act to erode the available potential energy. The procedure for the computations of the divergent kinetic energy is described in the next section.

The local change of available potential energy is small, implying that what is enhanced by the generation is passed on to the divergent kinetic energy by the divergent circulations. The magnitude of the generation is 47.3 units, whereas the conversion to the divergent kinetic energy is around 55.8 units. This implies that roughly 8.7 units are imported from the lateral boundaries.

The local change of the divergent kinetic energy is also small. Out of 55.8 units of divergent kinetic energy

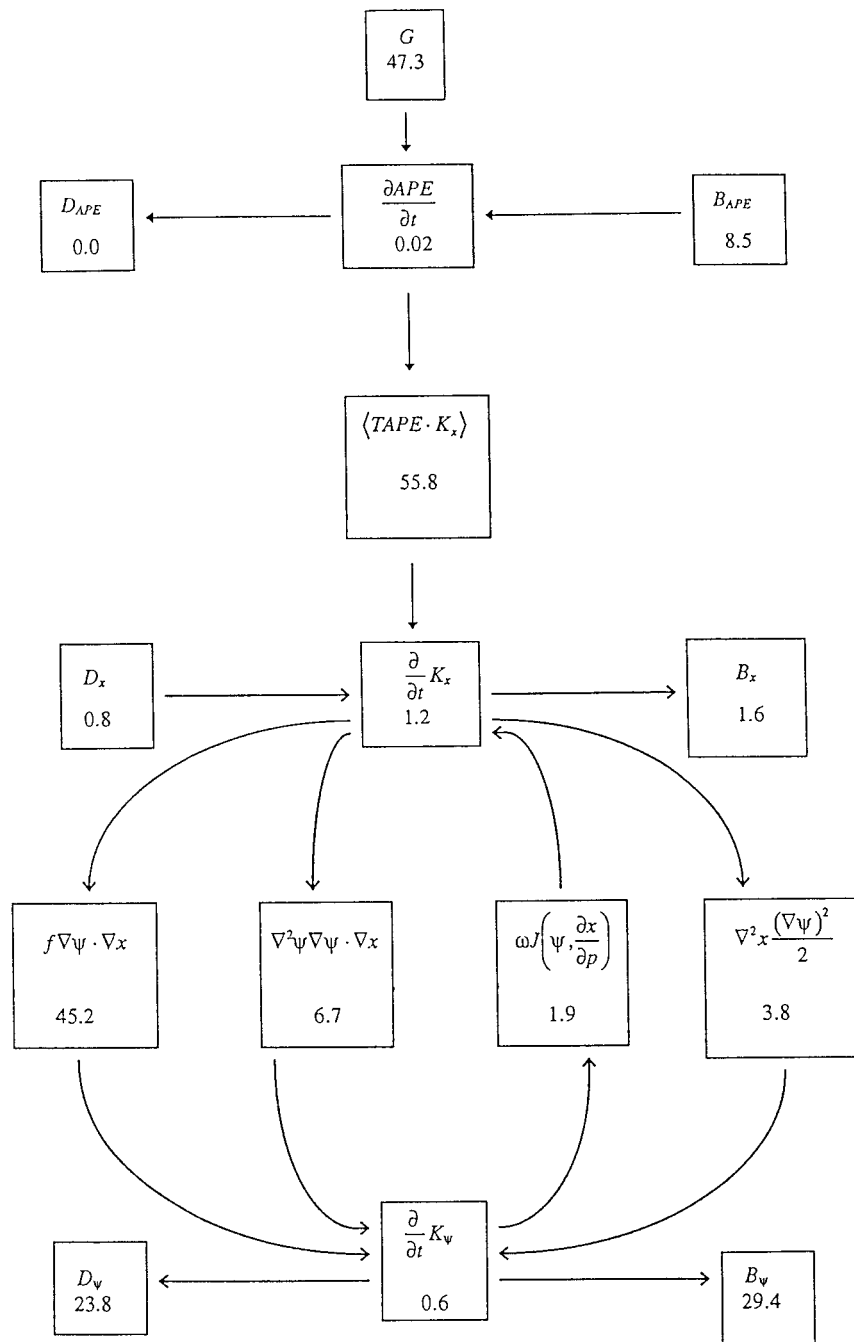


FIG. 5. Monsoon energetics. The various boxes denote different energy exchanges and their time rates of change in units  $10^{-5} \text{ m}^2 \text{ s}^{-3}$ . These are mean values over the domain  $30^\circ\text{S}$ – $40^\circ\text{N}$ ,  $30^\circ$ – $150^\circ\text{E}$  and 100 to 1000 hPa for the period 2–7 August 1979 based on a high-resolution global model forecast.

generated by vertical circulations the total amount transferred to the rotational kinetic energy is around 54.2 units. Thus boundary fluxes contribute to a small export of roughly 1.6 units of divergent kinetic energy. Four boxes (the second row from the bottom) illustrate the components of the  $\psi$ – $\chi$  interactions, [Eq. (13)]. Among

these four terms, the most significant of the  $\psi$ – $\chi$  interactions is the covariance  $f\nabla\psi\cdot\nabla\chi$ , which transfers 45.2 units from the divergent to the rotational kinetic energy. Again the local change of the rotational kinetic energy during this 6-day period was small. Most of the energy passed on to the rotational motions is either advected

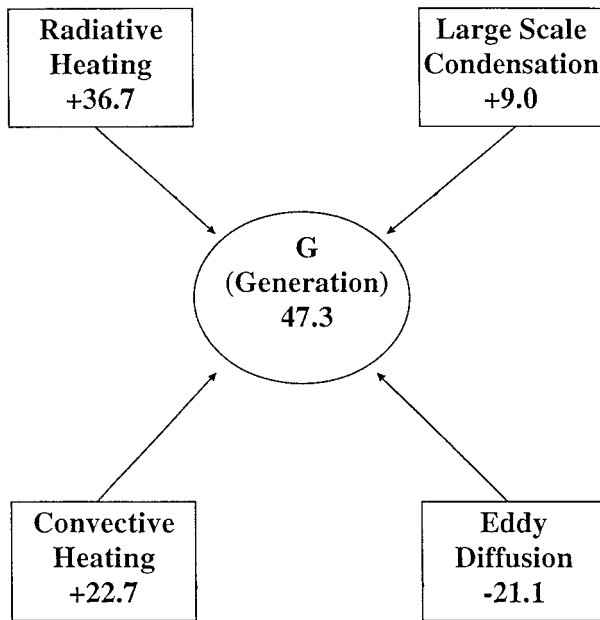


FIG. 6. Components of overall generation for the whole domain for the period 2–7 August 1979. Units  $10^{-5} \text{ m}^2 \text{ s}^{-3}$ .

out of the boundaries (roughly 30 units) or dissipated within this monsoon domain (roughly 24 units).

Overall, the message that emerges from Figs. 5 and 6 is that over the Indian monsoon regions the following is true.

- A substantial generation of available potential energy occurs during a period of steady and strong monsoon activity. This is enhanced by an additional import of available potential energy by about 20% from the lateral boundaries.
- The size of the monsoonal divergent circulations is very large (Krishnamurti 1985). Almost no import of divergent kinetic energy was necessary for the balance over the Indian monsoon domain.
- Almost all of the energy received by the divergent motions is passed on to the rotational kinetic energy. This transfer occurs from  $\psi$ – $\chi$  interactions largely from the preferred orientation of the  $\nabla\psi$  and  $\nabla\chi$  vectors.
- Finally, in this near-steady-state monsoon situation about half of the energy received by rotational motions is exported out of the monsoon domain. A substantial dissipation of the rotational kinetic energy is also evident over the Indian monsoon domain.

#### c. Energy conversions from vertical circulation

Vertical circulations can be viewed on the scale of the Hadley cell and on the scales of the eddy motions. Here we have combined these zonal and eddy contributions to examine the distributions of the conversion of total potential energy to the divergent kinetic energy,

Fig. 7. Figure 7 shows vertically integrated values over the entire troposphere for the 6-day period 2–7 August 1979. Basically we see large contributions to the conversion from available potential to divergent kinetic energy in the monsoon rainfall belt roughly north of  $20^\circ\text{N}$  and east of  $70^\circ\text{E}$ . Large conversions are also evident in the belt of midlatitude westerlies of the Southern Hemisphere south of  $25^\circ\text{S}$ .

The energy conversion terms are fairly standard (Lorentz 1967; Krishnamurti and Ramanathan 1982). Covariances among vertical velocity and temperature and those among the gradients of the streamfunction and the velocity potential are some of the salient components. The largest contribution to these conversions are generally found in the upper troposphere near 300 hPa. Figure 8 illustrates the contribution at 300 hPa for 7 August. The 300-hPa surface usually carries the best information on this energy exchange process since the warm core of the monsoon resides close to this level. Furthermore, the upward vertical motion is sufficiently large at this level to provide a maximum for this covariance at this level. Basically what we see in Figs. 7 and 8 is the dominance of the thermally direct circulations (shaded areas). As a consequence, the covariance of  $-\overline{\omega'T'}$  comes out positive, thus transferring available potential energy to kinetic energy of the divergent motions. Note also that available potential energy does not directly get transferred to rotational kinetic energy of the monsoon. The predicted temperature and vertical velocity fields for days 1, 3, and 5 for these forecasts were examined (not shown). They show an axis of warm upper-tropospheric temperature extends zonally along the latitude belt  $20^\circ$  to  $25^\circ\text{N}$ . This is the monsoonal warm core that has an amplitude of roughly 252 K ( $-21^\circ\text{C}$ ). Colder temperatures reside south of  $20^\circ\text{S}$ . The field of vertical velocity at 300 hPa was very cellular. Large upward motions of the order of  $-10^{-3}$  to  $-4 \times 10^{-3} \text{ hPa s}^{-1}$  were noted over the Bay of Bengal and the mountainous region to its north, and over the western Pacific Ocean. Downward motions were prevalent south of the equator. Large contributions are found over the heavy rain areas of the monsoon and the typhoons of the western Pacific Ocean. These are regions where rising motions and warm thermal anomalies coexist at 300 hPa.

#### d. The generation of available potential energy

The total generation shown in Figs. 9a,b includes the contributions from both the zonally averaged heating and the eddy components. Over the monsoon belt, the dominant forcing is that from the local Hadley cell with heating north of  $15^\circ\text{N}$ , where the tropospheric temperatures are warm, and cooling south of  $5^\circ\text{S}$ , where the tropospheric temperatures are cold. Largely negative values of the generation are only noted over the equatorial belt between  $5^\circ\text{S}$  and  $10^\circ\text{N}$ . During the 6-day period of this forecast the largest values of the generation

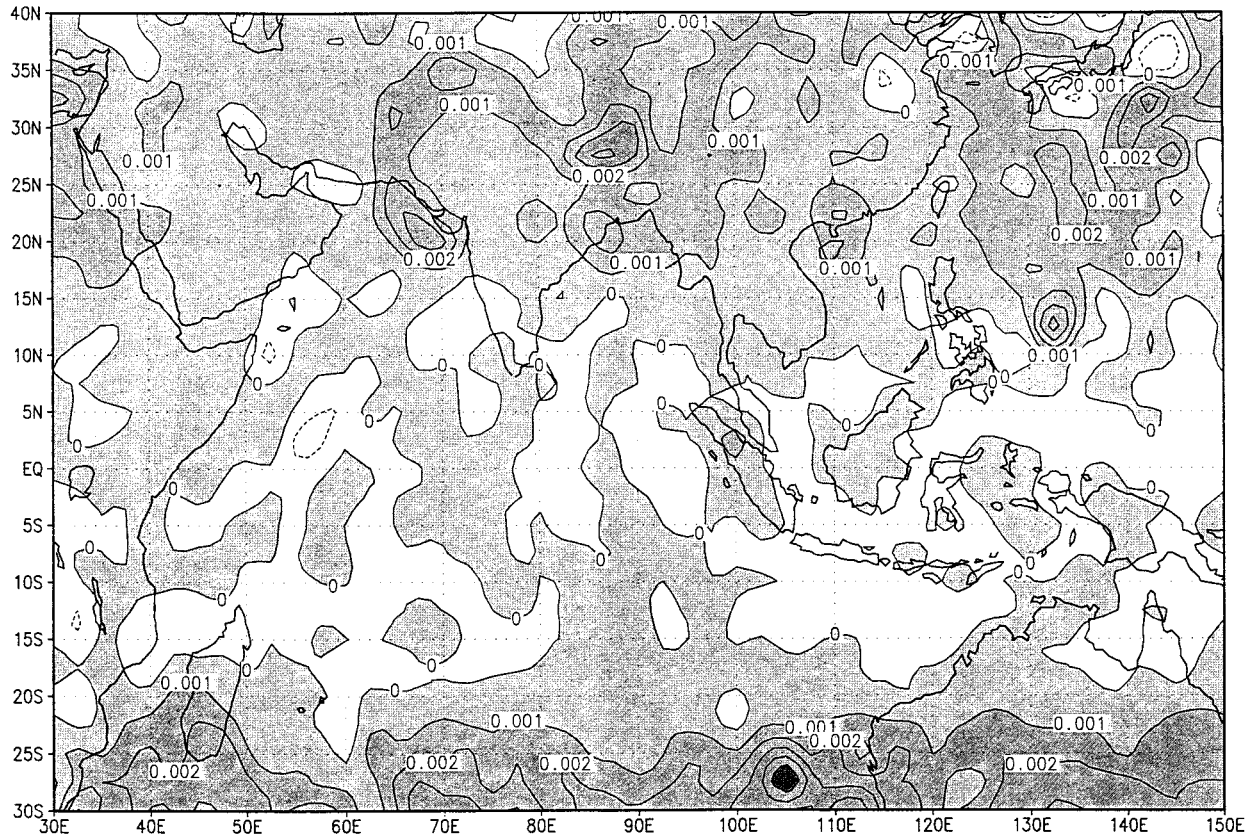
Mean  $w^1 T^1$  ( $m^2 s^{-3}$ ) 12Z Aug. 2-7, 1979

FIG. 7. Vertically integrated product  $-\omega^1 T^1$ , averaged for the period 2-7 August 1979. Units:  $m^2 s^{-3}$ .

occurred over the Tibetan Plateau. Western China was characterized by warm tropospheric temperatures and rain-free conditions. The conspicuous negative generation over this region was related to the radiative cooling. On the whole, the distribution of generation was quite similar for an individual day, 5 August, as they were for the entire week (Figs. 9a,b). On 5 August an upper trough was located near  $110^\circ E$  and north of  $30^\circ N$ . The descending air to the west of this upper trough was over a relatively rain-free region. The negative generation was quite pronounced on this date and was clearly related to the synoptic setting.

Luo and Yanai (1983) have examined in detail the distribution of heating during the monsoon over different regions. Our results are essentially consistent with their findings.

The heat low over the Saudi Arabian peninsula is another region where a maximum value of the net generation is found (Blake et al. 1983). The magnitude of this maximum value is less than that found over the active monsoon regions. We have examined the vertical distribution of the generation term over this region and found that most of the contribution over the Saudi Arabian peninsula is produced by the atmosphere below

850 hPa. That contribution evidently comes from the Saudi Arabia heat low, where a strong surface heating occurs over the warm surface layer.

#### e. The $\psi$ - $\chi$ interactions

Here we shall illustrate the  $\psi$ - $\chi$  interactions of this forecast at 850 hPa. Figures 10a-c illustrates these (respectively) for days 1, 3, and 5 of the forecast. Each panel includes two sets of vector fields; the blue vector shows the rotational motion field  $\mathbf{k} \times \nabla \psi$ , the red vector denotes the divergent wind, and the green and yellow isopleths show the transfer of kinetic energy from the divergent to the rotational motions. In order to appreciate the salient energy transfer function  $f \nabla \psi \cdot \nabla \chi$ , one first needs to look at regions where strong values of the rotational and divergent wind coexist and where these are more nearly normal to each other. A counterclockwise turn from the rotational flow to the divergent flow (turn close to  $90^\circ$ ) favors the maximum exchange from the divergent to the rotational flow. A similar clockwise turn signifies an exchange of energy from the rotational to the divergent flow.

During this period, one of the most active regions

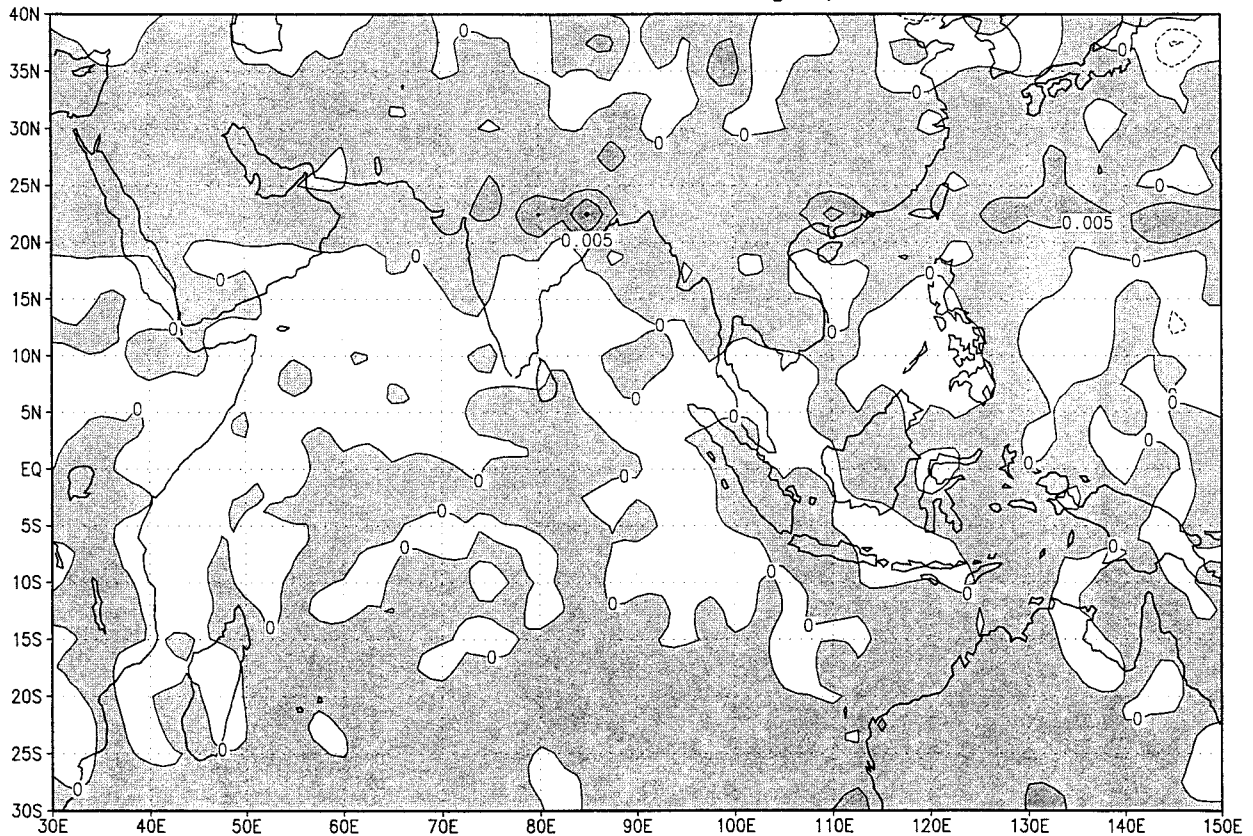
300 MB  $w'T'$  ( $\text{m}^2 \text{s}^{-3}$ ) 12Z Aug. 7, 1979

FIG. 8. Product  $-\omega'T'$  at 300 hPa in units  $\text{m}^2 \text{s}^{-3}$  for day 5 (7 August 1979, 1200 UTC).

where large contributions to the energy exchange from the divergent to the rotational motions occur lies over the northern Arabian Sea along the Somali jet. The Somali jet reveals some of the strongest nongeostrophic and divergent motions along its traverse over the Arabian Sea. The ratio of the amplitudes of the divergent to the rotational wind is around 0.2–0.25 in this region at 850 hPa. As the first monsoon depression moved westward, the converging flow into this disturbance contributed to the enhancement of the energy exchange from the divergent to the rotational wind. This happens because the evolving  $\nabla_\chi$  happens to be normal to the  $\nabla_\psi$  field. A positive feedback is noted and this leads to further enhancement of the rotational flow of the disturbance. During this period we can see a substantial growth of the energy exchange  $\langle K_\chi, K_\psi \rangle$  over the Arabian Sea and southern India to the south of the disturbance.

In the upper troposphere as well a substantial transfer of energy from the divergent to the rotational flow occurs over this region. These vectors at 200 hPa also clearly demonstrate a near-normal relationship; that is,  $\nabla_\psi$  is normal to  $\nabla_\chi$  (not shown here). There are a few other regions where the values of this energy exchange are large, but they do not exhibit the same degree of

steady behavior as the Somali jet. Modeling of the monsoon clearly requires that the details of the divergent and the rotational wind are properly simulated.

#### f. Vertical distribution of major covariances

In the monsoon energetics the major covariances are the following:

- 1)  $\langle H'T' \rangle$  heating rates and temperature,
- 2)  $-\langle \omega'T' \rangle$  vertical velocity and temperature, and
- 3)  $f\nabla\psi \cdot \nabla\chi$  energy exchange from the divergent to the rotational component.

The vertical distributions of these covariances show some interesting features. Figures 11a–c show the vertical distribution of these covariances (respectively) during the 5-day forecast of the active monsoon. In this illustration the different curves show the net generation for the different days during 2–7 August, 1979. These integrations are area averaged over the entire domain between 30°–150°E and 30°S–40°N. The covariance of heating and temperature exhibits a maximum value in the upper troposphere near 200 hPa. This maximum arises from heating over the warm upper troposphere

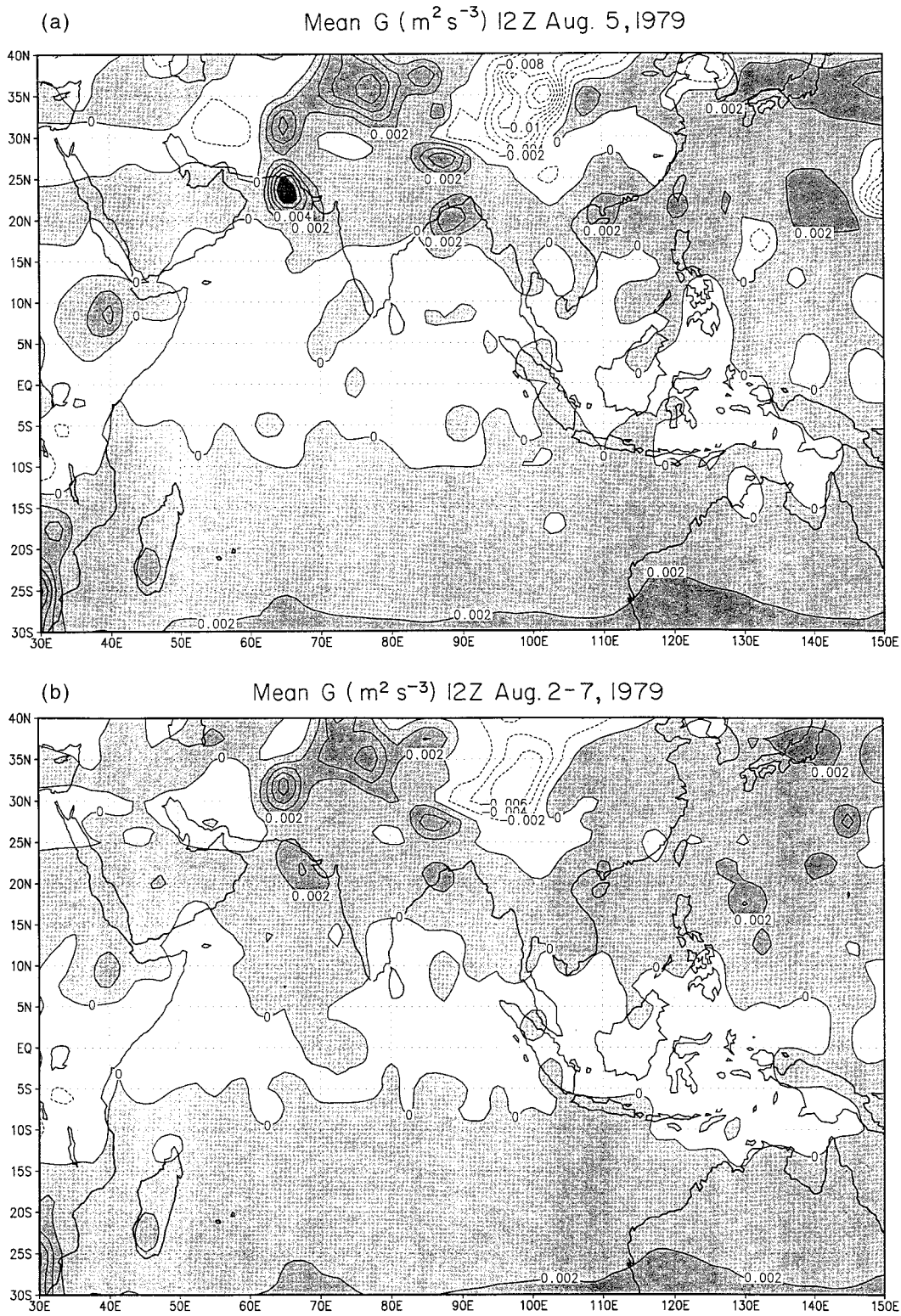


FIG. 9. Distribution of the generation of total available potential energy. These are vertically integrated between 100 and 1000 hPa. Units:  $m^2 s^{-3}$ . (a) For 5 August 1979 at 1200 UTC. (b) Mean for period 2-7 August 1979.

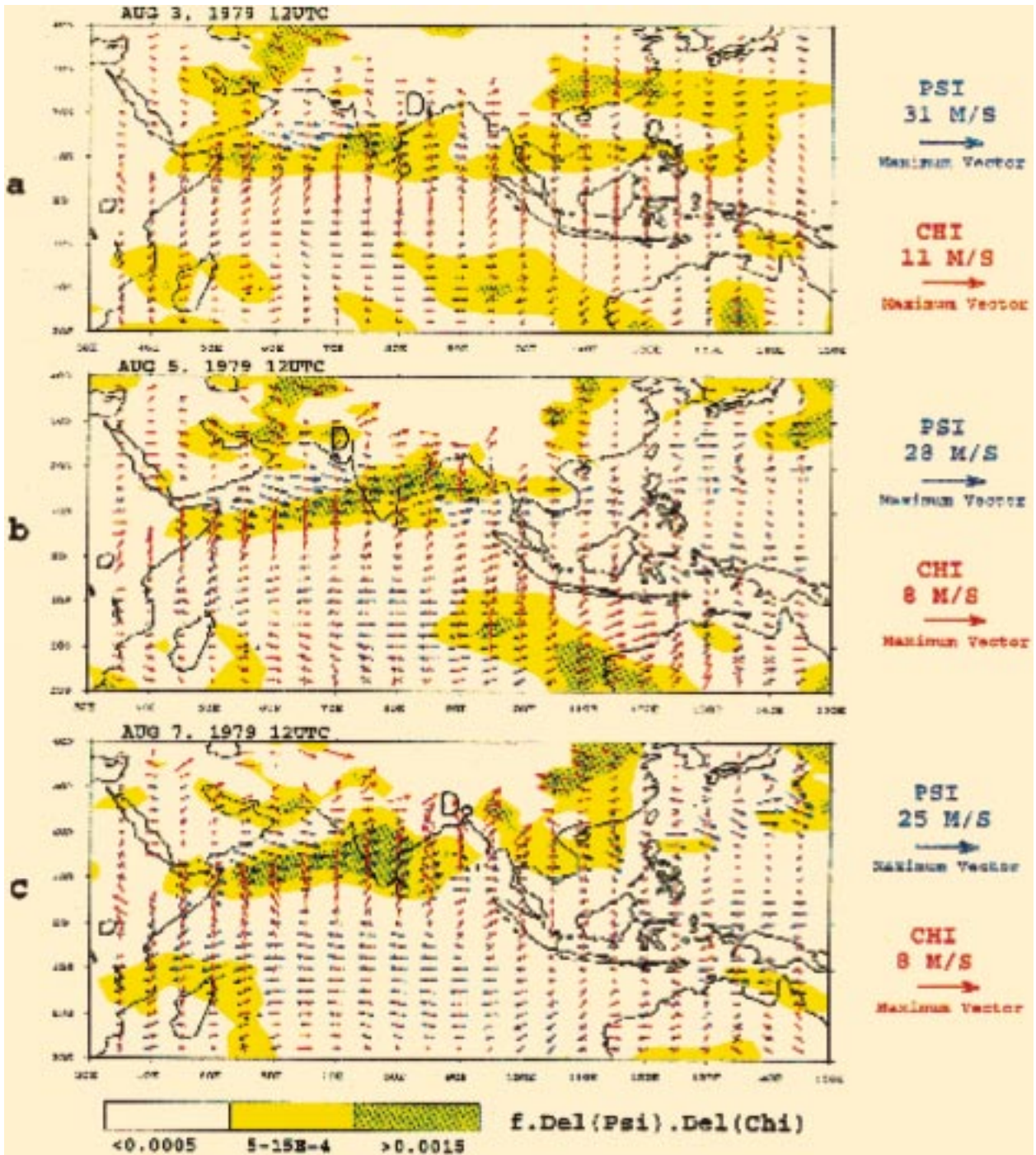


FIG. 10. 850-hPa rotational wind vectors (blue), the divergent wind vectors (red), and the field of the energy exchange from the divergent to the rotational kinetic energy (green and yellow following the scale shown below). Units of wind  $\text{m s}^{-1}$ , energy exchange  $\text{m}^2 \text{s}^{-3}$ . The different panels denote results for days 1, 3, and 5 of forecast. (a) 3 August 1979, 1200 UTC. (b) 5 August 1979, 1200 UTC. (c) 7 August 1979, 1200 UTC.

and is related to deep cumulus convection [see also Luo and Yanai (1983)]. Most of the generation of available potential energy for the driving of the monsoon comes from convection over the warm land mass and radiative cooling over the Southern Ocean where the upper tro-

posphere is cooler. The radiative cooling profiles exhibit tropospheric rates of roughly  $2^\circ\text{C day}^{-1}$ . In Fig. 11a we find an essential bimodal distribution of the net generation over the Indian monsoon domain. This bimodality is explained later in Figs. 12a,b. The radiative

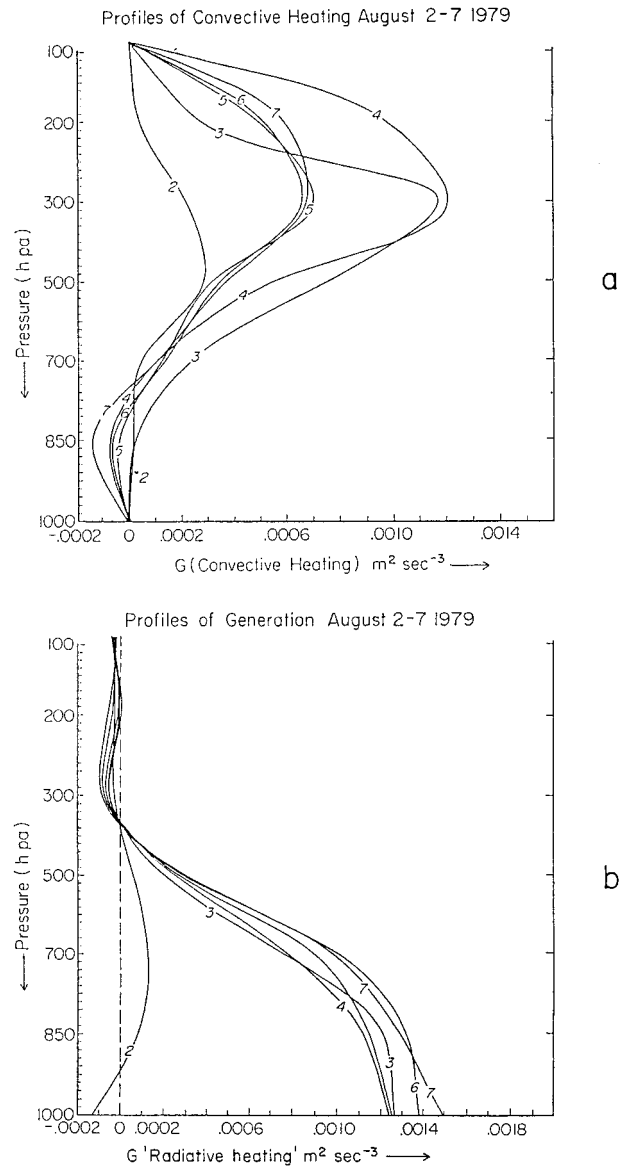
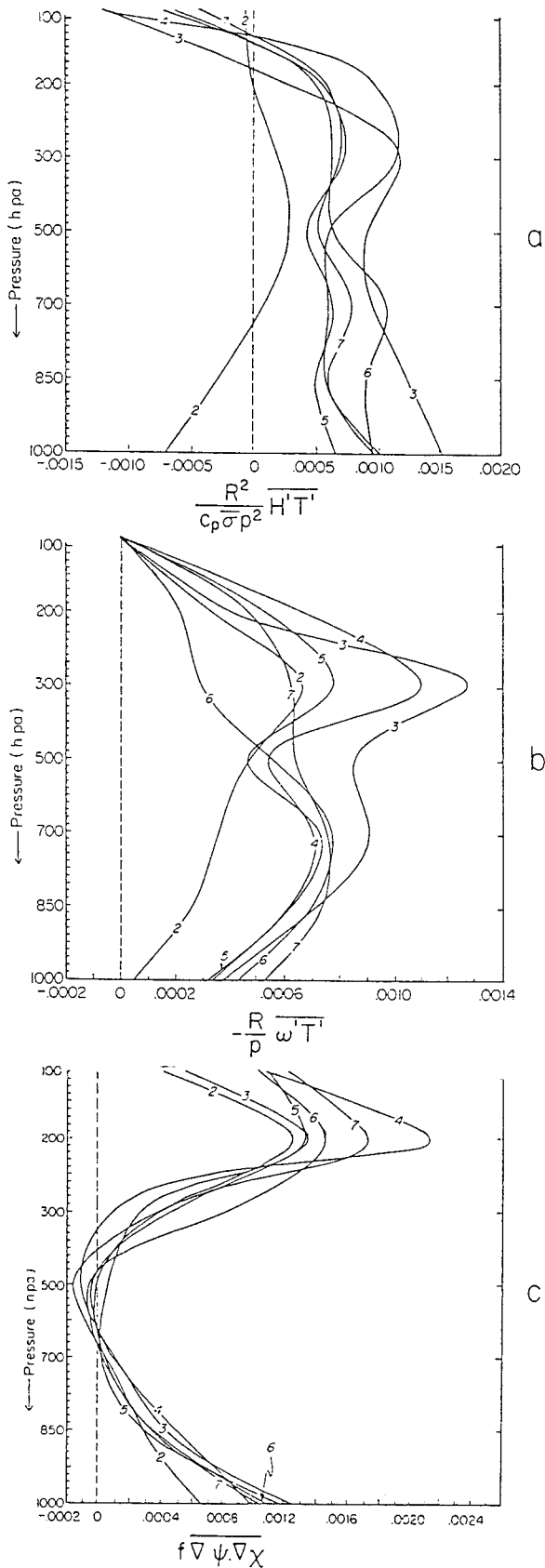


FIG. 12. Vertical profiles of the contributions to the generations of available potential energy. Domain averaged over 30°–150°E, 30°S–40°N. (a) Convective heating, (b) radiative forcing. Units: 10 m<sup>2</sup> s<sup>-3</sup>. Labels on curves show dates of forecasts from 2 to 7 August 1979, 1200 UTC.

flux convergence contributes toward the lower-tropospheric maximum and the convective component contributes over the upper troposphere.

The vertical distribution of the covariance of vertical

FIG. 11. Vertical distribution of the covariances of energy quantities. Averaged over the domain 30°–150°E, 30°S–40°N and for individual days (as marked) for the period 2–7 August 1979. (All units m<sup>2</sup> s<sup>-3</sup>). (a) Heating and temperature ( $\overline{H'T'}$ ); (b) Vertical velocity and temperature ( $\overline{-w'T'}$ ); (c)  $\psi$ - $\chi$  interaction ( $\overline{f \nabla \psi \cdot \nabla \chi}$ ).

velocity and temperature is shown in Fig. 11b. Here we show the plots of  $-\overline{\omega'T'}$  as a function of forecast day for this active monsoon spell. This covariance also exhibits a maximum in the lower and upper troposphere. These features are largely related to the location of the maximum upward motion of the convective rain area. That seems to occur close to the 300- and the 700-hPa surfaces. The excessive monsoon rainfall over the subcontinent is partly due to tall orographic cumulonimbus clouds and a plethora of nimbostratus clouds whose tops are below 500 hPa. The bimodality of the vertical profile of  $-\overline{\omega'T'}$  is evidently enhanced by both of these types. The lower-tropospheric maximum is also a result of descending regions where the maximum contribution to the covariance of  $-\overline{\omega'T'}$  is large. The day-to-day variability during a 5-day forecast is not very large and the forecasts on all days essentially describe the same features. This essentially confirms that available potential energy generated by differential heating is being passed on to divergent kinetic energy. The largest contributor to the exchange of divergent to rotational kinetic energy arises from the covariance  $\langle f\nabla\psi \cdot \nabla\chi \rangle$ , which has a bimodal vertical distribution. A strong maxima in the upper troposphere and a weaker maximum in the lower troposphere are found (Fig. 11c). Again the forecast of a fully developed monsoon exhibits a robustness of these results from one day to the next. A preferred orientation of the  $\psi$  and  $\chi$  isopleths with respect to each other provides a large (nonzero) value for the dot product of  $\nabla\psi$  and  $\nabla\chi$ . That is best seen from  $V_\psi$ ,  $V_\chi$ , and  $f\nabla\psi \cdot \nabla\chi$  at 850 hPa in Figs. 10a–c. It is clearer if one first looks at the maxima in the field of  $f\nabla\psi \cdot \nabla\chi$ . Those locations show the orientation of  $\nabla\psi$  and  $\nabla\chi$ . It is apparent that the mature monsoon exhibits a preferred orientation of the  $V_\psi$  and  $V_\chi$  isopleths, thus facilitating a transfer of energy from the divergent to the rotational kinetic energy. These features are most pronounced in the trades, the Somali jet, and the southwest monsoon over central India, which extends to the coast of China.

The contribution to the generation term from different components of heating can be easily calculated noting that

$$\overline{H'T'} = \overline{\left( \sum H_i \right) T'},$$

where  $H_i$  denotes the individual components. Among the several components of diabatic heating, the covariance from cumulus-scale heating and the radiative forcing were the two largest terms. The horizontally area averaged ( $30^\circ$ – $150^\circ$ E and  $30^\circ$ S– $40^\circ$ N) contribution from these two terms is shown in Figs. 12a,b. Here we show the vertical profiles of these contributions to the generation terms for the individual days during 2–7 August 1979. The largest generation of available potential energy from cumulus convection occurs near 300 hPa (Fig. 12a). Evidently on one of those days convective heating prevailed away from the warmest tropospheric thermal

field. Below 600 hPa a small negative value of the generation from the convective component is related to the covariance of heating and relatively colder lower-tropospheric temperatures. A closer inspection of the thermal field reveals that the warmest lower-tropospheric temperature resides over the heat lows that are devoid of convective heating. A substantial generation of available potential energy from the radiative heating is seen on most days around 700 hPa (Fig. 12b). This is related to the net radiative cooling on top of the moist layer and the shallow stratocumulus clouds. A secondary weak generation is also noted over the tropical upper troposphere. Radiative flux convergence below the tops of the tall cumulonimbus anvils (as seen by the model's humidity profiles) over regions of warm tropospheric temperatures of the monsoon rain belt contributes to this feature. The forecasts for 2 August are consistent with respect to the energy conversions and the generation terms illustrated in Figs. 11 and 12.

## 5. Concluding remarks

By selecting a period of active near-steady monsoon during the FGGE/MONEX year 1979 we have exploited the datasets from a high-resolution global forecast to carry out computations of monsoon energetics. The success of the forecast in terms of circulation and precipitation enabled us to use consistent data for this study. Two major theoretical factors provided insights in our interpretations on the maintenance of the monsoon. By casting the basic equations in the framework of rotational and divergent motions, it was possible to note that vertical divergent circulations transfer available potential energy directly to the energy of divergent motions. Both the Hadley and the Walker circulations are divergent circulations on the meridional and the zonal vertical sections. Through ascent of relatively warmer air and descent of relatively colder air they transfer available potential energies to the kinetic energy of these divergent motions. The other insight came from the recognition that the orientation of the isopleths of the streamfunction  $\psi$  and the velocity potential  $\chi$  play a major role in determining the transfer of divergent kinetic energy into that of rotational motions of the monsoon. In the Northern Hemisphere over a three-dimensional monsoon domain, it requires that the dot product of  $\nabla\psi$  and  $\nabla\chi$  be positive and large. We noted from the charts of  $\psi$  and  $\chi$  during the active monsoon spell that such is the case. Thus the monsoon engine, viewed in the context of rotational and divergent motions, appears to provide a link between the heat sources, sinks, and the eventual maintenance.

In this paper we have addressed the issue of the maintenance of the Indian monsoon. Over a selected domain of the Indian monsoon we have shown a near steady state in the temporal change of various domain averaged quantities such as rotational and divergent kinetic energy and available potential energy. The maintenance

of the Indian monsoon component appears to also rely on the import and export of energy into this open system.

The aforementioned results came from a medium-range numerical weather prediction experiment that was carried out with a global model at high resolution. The results, no doubt, are sensitive to the physical parameterizations used in the model. Further refinements in the model dynamics, physics, and representation of orography will of course refine these results further. Use of analyzed model-assimilated datasets must also suffer from the same problems; that is, any heat budget must reflect the physical parameterization of the modeled heat sources and sinks. Budgets devoid of modeling approximations are hard to carry out for large-scale weather systems. This type of modeling of the monsoons evidently requires the proper simulations of the phases of the heating components, the temperature field, the vertical velocity, and the geometries of the rotational and divergent wind components. Errors in these fields arise from initial data descriptions and from the entire array of modeling approximations and formulations. Perhaps the most revealing aspect of this formulation is that the pressure interactions in the energy equation ( $v \cdot \nabla \times z$ ) is zero, thus making it possible to interpret the three-dimensional monsoon in the same way as one does for the zonally symmetric monsoon. That decoupling is only possible if one writes these energy equations in the framework of the rotational and divergent motions. The orientation of the  $\nabla\psi$  and  $\nabla\chi$  isopleths is very important; degradation of these fields leads to a weakening of the transfer of kinetic energy for the maintenance of the monsoon. These orientations are a strong function of the physics of the global model. Cumulus convection over the heat source of the monsoonal land mass and the radiative cooling over the southern ocean generate these divergent and rotational motions. The efficient transfer of energy among the rotational and divergent wind components requires that the vectors  $\nabla\psi$  and  $\nabla\chi$  are nearly perpendicular. We were able to simulate that feature in our forecast.

*Acknowledgments.* This work was supported by NSF Grant ATM9312537 and NOAA Grant NA56GP0013. Computations for this work were carried out at the NSF supercomputer center, San Diego.

#### APPENDIX A

##### $\psi$ - $\chi$ Interactions

The horizontal wind is decomposed into the usual rotational and divergent wind by the relation

$$V = \mathbf{k} \times \nabla\psi - \nabla\chi.$$

The rotational kinetic energy equation is expressed by

$$\begin{aligned} \frac{\partial \overline{\overline{K_\psi}}}{\partial t} &= \overline{\overline{f \nabla\psi \cdot \nabla\chi}} + \overline{\overline{\nabla^2 \chi \frac{|\nabla\psi|^2}{2}}} + \overline{\overline{\nabla^2 \psi \nabla\psi \cdot \nabla\chi}} \\ &+ \omega J\left(\psi, \frac{\partial\chi}{\partial p}\right) + \overline{\overline{D_\psi}} + B_\psi. \end{aligned}$$

The divergent kinetic energy equation is expressed by

$$\begin{aligned} \frac{\partial \overline{\overline{K_\chi}}}{\partial t} &= \overline{\overline{-\chi \nabla^2 \theta}} - \overline{\overline{f \nabla\psi \cdot \nabla\chi}} - \overline{\overline{\nabla^2 \psi (\nabla\psi \cdot \nabla\chi)}} \\ &- \overline{\overline{\nabla^2 \chi \frac{|\nabla\psi|^2}{2}}} - \omega J\left(\psi, \frac{\partial\chi}{\partial p}\right) + \overline{\overline{D_\chi}} + B_\chi. \end{aligned}$$

The equation for available potential energy is expressed by

$$\frac{\partial \overline{\overline{\text{APE}}}}{\partial t} = \overline{\overline{\chi \nabla^2 \phi}} + \overline{\overline{G}} + \overline{\overline{D_{\text{APE}}}} + B_{\text{APE}}.$$

The boundary flux term in the rotational kinetic energy equation is given by

$$\begin{aligned} B_\psi &\equiv \nabla \cdot \left( \psi \nabla \frac{\partial\psi}{\partial t} \right) + J\left(\frac{\psi^2}{2}, \nabla^2 \psi + f\right) - J\left(\omega\psi, \frac{\partial\chi}{\partial p}\right) \\ &+ \nabla \cdot \left( \psi \omega \frac{\partial}{\partial p} \nabla\psi \right) - \frac{\partial}{\partial p} \omega \frac{|\nabla\psi|^2}{2}. \end{aligned}$$

The boundary flux term in the divergent kinetic energy equation is given by

$$\begin{aligned} B_\chi &\equiv \nabla \cdot \left( \chi \frac{\partial\psi}{\partial t} \nabla\chi \right) + J\left(\frac{\chi^2}{2}, \nabla^2 \psi + f\right) - J\left(\omega\chi, \frac{\partial\chi}{\partial p}\right) \\ &- \nabla \cdot \left\{ \chi \nabla \left[ \frac{|\nabla\psi|^2}{2} + \frac{|\nabla\chi|^2}{2} - J(\psi, \chi) \right] \right. \\ &\quad \left. - \nabla\chi \left[ \frac{|\nabla\psi|^2}{2} + \frac{|\nabla\chi|^2}{2} - J(\psi, \chi) \right] \right\} \\ &- \frac{\partial}{\partial p} \left\{ \omega \left[ \frac{|\nabla\psi|^2}{2} - J(\psi, \chi) \right] \right\} \\ &+ \nabla \cdot \left\{ \chi \nabla\psi (\nabla^2 \psi + f) + \chi \omega \frac{\partial}{\partial p} \nabla\chi \right\}. \end{aligned}$$

#### APPENDIX B

##### Outline of the FSU Global Spectral Model

The global model used in this study is identical to that used in Krishnamurti et al. (1991). The following is an outline of the global model.

- 1) Independent variables: ( $x, y, \sigma, t$ ).
- 2) Dependent variables: vorticity, divergence, surface pressure, vertical velocity, temperature, and humidity.

- 3) Horizontal resolution: triangular 170 waves.
- 4) Vertical resolution: 15 layers between roughly 10 and 1000 mb.
- 5) Semi-implicit time-differencing scheme.
- 6) Envelope orography (Wallace et al. 1983).
- 7) Centered differences in the vertical for all variables except humidity, which is handled by an upstream differencing scheme.
- 8) Fourth-order horizontal diffusion (Kanamitsu et al. 1983).
- 9) Kuo-type cumulus parameterization (Krishnamurti et al. 1983a).
- 10) Shallow convection (Tiedke 1984).
- 11) Dry convective adjustment.
- 12) Large-scale condensation (Kanamitsu 1975).
- 13) Surface fluxes via similarity theory (Businger et al. 1971).
- 14) Vertical distribution of fluxes utilizing diffusive formulation where the exchange coefficients are functions of the Richardson number (Louis 1979).
- 15) Long- and shortwave radiative fluxes based on a band model (Harshvardan and Corsetti 1984; Lacis and Hansen 1974).
- 16) Diurnal cycle.
- 17) Parameterization of low, middle, and high clouds based on threshold relative humidity for radiative transfer calculations
- 18) Surface energy balance coupled to the similarity theory (Krishnamurti et al. 1991)
- 19) Nonlinear normal mode initialization – 5 vertical modes (Kitade 1983).
- 20) Physical initialization (Krishnamurti et al. 1991).

## REFERENCES

- Blake, D. W., T. N. Krishnamurti, S. V. Low-Nam, and J. S. Fein, 1983: Heat low over the Saudi Arabian Desert during May 1979 (Summer MONEX). *Mon. Wea. Rev.*, **111**, 1759–1775.
- Businger, J. A., J. C. Wyngard, Y. Izumi, and E. F. Bradley, 1971: Flux profile relationship in the atmospheric surface layer. *J. Atmos. Sci.*, **28**, 181–189.
- Harshvardan, and T. G. Corsetti, 1984: Longwave parameterization for the UCLA/GLAS GCM. NASA Tech. Memo. 86072, 52 pp. [Available from NASA/Goddard Space Flight Center, Greenbelt, MD 20771.]
- Kanamitsu, M., 1975: On numerical prediction over a global tropical belt. Rep. 75-1, Dept. of Meteorology, The Florida State University, 282 pp. [Available from The Florida State University, Tallahassee, FL 32306.]
- , K. Tada, K. Kudo, N. Sato, and S. Ita, 1983: Description of the JMA operational spectral model. *J. Meteor. Soc. Japan*, **61**, 812–828.
- Kitade, T., 1983: Nonlinear normal mode initialization with physics. *Mon. Wea. Rev.*, **111**, 2194–2213.
- Krishnamurti, T. N., 1985: Summer Monsoon Experiment—A review. *Mon. Wea. Rev.*, **113**, 1590–1626.
- , and H. Bhalme, 1976: Oscillations of a monsoon system. Part I: Observational aspects. *J. Atmos. Sci.*, **33**, 1937–1954.
- , and R. Ramanathan, 1982: Sensitivity of monsoon onset to differential heating. *J. Atmos. Sci.*, **39**, 1290–1306.
- , and D. Oosterhof, 1989: Prediction of the life cycle of a super typhoon with a high resolution global model. *Bull. Amer. Meteor. Soc.*, **70**, 1218–1230.
- , S. Low-Nam, and R. Pasch, 1983a: Cumulus parameterization and rainfall rates II. *Mon. Wea. Rev.*, **111**, 816–828.
- , S. Cocks, R. Pasch, and S. Low-Nam, 1983b: Precipitation estimates from raingauge and satellite observations summer MONEX. Rep. 83-7, Department of Meteorology, The Florida State University, 373 pp. [Available from The Florida State University, Tallahassee, FL 32306.]
- , H. S. Bedi, and D. K. Oosterhof, 1990: Precipitation prediction over the tropics from a global spectral model. *Atmósfera*, **3**, 255–280.
- , J. Xue, H. S. Bedi, K. Ingles, and D. Oosterhof, 1991: Physical initialization for numerical weather prediction over the tropics. *Tellus*, **43AB**, 53–81.
- , H. S. Bedi, and K. Ingles, 1993: Physical initialization using SSM/I rain rates. *Tellus*, **45A**, 247–269.
- , G. D. Rohaly, and H. S. Bedi, 1994: On the improvement of precipitation forecast skill from physical initialization. *Tellus*, **46A**, 598–614.
- Lacis, A. A., and J. E. Hansen, 1974: A parameterization for the absorption of solar radiation in the earth's atmosphere. *J. Atmos. Sci.*, **31**, 118–133.
- Lorenz, E. N., 1967: *The Nature and Theory of the General Circulation of the Atmosphere*. World Meteorological Organization, 161 pp.
- Louis, J. F., 1979: A parametric model of vertical eddy fluxes in the atmosphere. *Bound.-Layer Meteor.*, **17**, 187–202.
- Luo, H., and M. Yanai, 1983: The large-scale circulation and heat sources over the Tibetan plateau and surrounding areas during the early summer of 1979. Part I: Precipitation and kinetic analyses. *Mon. Wea. Rev.*, **111**, 922–977.
- Murakami, T., R. V. Godbole, and R. R. Kelkar, 1970: Numerical simulation along 80°E. *Proc. Conf. on the Summer Monsoon of Southeast Asia*, Norfolk, VA, Navy Weather Research Facility, 39–51.
- Ogura, Y., and M. Yoshizaki, 1988: Numerical study of orographic-convective precipitation over the eastern Arabian Sea and the Ghat Mountains during the summer monsoon. *J. Atmos. Sci.*, **45**, 2097–2122.
- Saltzman, B., 1970: Large scale atmospheric energetics in the wave number domain. *Rev. Geophys. Space Phys.*, **8**, 289–302.
- Smith, R. B., and Y. Lin, 1983: Orographic rain on the western Ghats. *The Forcings of the First Sino-American Workshop on Mountain Meteorology*, E. Reiter, Z. Baozhen, and Q. Yongfu, Eds., Science Press and Amer. Meteor. Soc., 71–94.
- Tiedtke, M., 1984: The sensitivity of the time-mean large-scale flow to cumulus convection in the ECMWF model. *Proc. Workshop on Convection in Large-Scale Numerical Models*, Reading, United Kingdom, ECMWF, 297–316.
- Wallace, J. M., S. Tibaldi, and A. J. Simmons, 1983: Reduction of systematic forecast errors in the ECMWF model through the introduction of envelope orography. *Quart. J. Roy. Meteor. Soc.*, **109**, 683–718.
- Wiin-Nielsen, A., and T. C. Chen, 1993: *Fundamentals of Atmospheric Energetics*. Oxford University Press, 376 pp.